PASSIVE BROADBAND HIGH DYNAMIC RANGE SEMICONDUCTOR LIMITERS

D.J. Hagan, E.W. Van Stryland, Y.Y. Wu, T.H. Wei, M. Sheik-Bahae,
A. Said, Kamjou Mansour, J. Young and M.J. Soileau.

Center for Research in Electro-Optics and Lasers
University of Central Florida, Orlando, FL 32826

ABSTRACT

The principles of operation of semiconductor optical limiters which utilize two-photon absorption and free-carrier induced defocusing are described. We present a review of early work using psec pulses at 532 nm in ZnSe, in which the problem of damage in solid state limiters is overcome by optimizing the focusing geometry. Limiting energies as low as 10 nJ are seen, and a dynamic range (damage energy divided by limiting energy) in excess of 10^4 is demonstrated. The somewhat complicated propagation theory is simplified into a set of scaling rules which are used to predict operating characteristics of semiconductor limiters at longer wavelengths and for shorter pulses. We present new limiting data obtained with longer pulses in ZnSe, in CdTe at 1.06 μm and InSb at 10.6 μm, and we compare these results with the scaling rules.

1. INTRODUCTION

Passive optical limiting results from irradiance-dependent nonlinear-optical processes in materials. [1,2] The ideal optical limiter has the characteristics shown in Figure 1. It has a high linear transmittance for low input (e.g., energy E or power P), a variable limiting input E or P, and a large dynamic range, defined as the ratio of E or P at which the device damages (irreversibly) to the limiting input. Since a primary application of the optical limiter is for protection of sensitive optical components such as detectors, and damage to detectors is normally determined by fluence, this is the quantity of interest for the output of the limiter. Getting the response of Figure 1 turns out to be possible by using a wide variety of materials; however, it is difficult to get the limiting threshold as low as is often required and at the same time to have a large dynamic range.

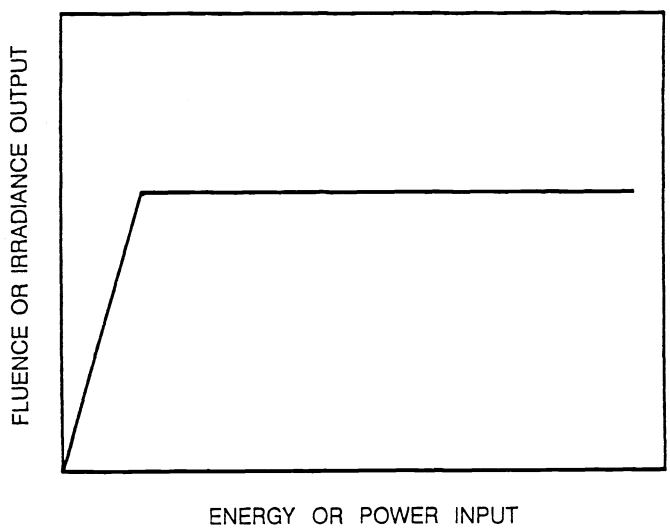

Fig. 1. Fluence output of an ideal optical limiter as a function of the input power or energy.

Because high transmittance for low inputs is desired, we must have low linear absorption. These criteria lead to the use of two-photon absorption (2PA) and nonlinear refraction. In this paper we present the detailed operational characteristics and a theoretical description of optical limiting devices based on 2PA and the subsequent photogenerated free-carrier defocusing in semiconductors.

2. HISTORICAL BACKGROUND

Semiconductors have exhibited some of the largest optical nonlinearities of all materials. [3] Unfortunately, from the standpoint of optical limiting, these extremely large nonlinearities are associated with near bandgap resonance and thus are in a region of relatively high linear absorption. In addition, solids undergo irreversible optical damage. Even so, effective limiting has been demonstrated by using other mechanisms. In 1969, Geusic *et al.* reported limiting behavior in Si attributed to stepwise nonlinear absorption at 1.06 μm. [4] Later, Boggess *et al.* showed fluence limiting in Si that was due to a combination of nonlinear absorption with a refractive contribution induced by the photoexcitation of free carriers. [5] Power-limiting experiments were conducted by Ralston and Chang in a series of semiconductors such as CdS, GaAs, and CdSe. [6] This was the first report to our knowledge of the use of 2PA for optical limiting. In those studies nanosecond pulses were used where absorption by the 2PA-generated free carriers was significant. In addition, although this was not noted at the time, the refractive index change caused by photo-generated carriers is strong and also useful in the limiting process. In particular, this defocusing limits the transmitted fluence. Another type of limiter, which uses a combination of 2PA and nonlinear refraction in the narrow gap semiconductor InSb at 10 μm, was developed by Walker et al. [7] This device relies on the etalon properties of the nonlinear sample, and the device exhibits regions of bistability, but the range of input energies over which limiting is obtained is small. Boggess et al. were the first to use the combined effects of 2PA and carrier defocusing to obtain optical fluence limiting. [8] The geometry used was to focus picosecond 1.06 μm pulses onto the surface of a thin sample of GaAs, refocus the beam, and monitor the transmittance of an aperture. Since the damage-prone surfaces are subjected to the maximum fluence of the input pulses, the range over which these devices function without incurring damage is low. What we have found is that if thick samples are used, the large nonlinearities of the semiconductor can actually be used to prevent damage. [9] The trick is simply to focus the light tightly into the bulk of the material. Nonlinear absorption combined with nonlinear refraction keeps the irradiance within the semiconductor below the damage threshold, and the device is self-protecting. One problem now is that the wave equation can no longer be separated into two propagation equations, one for the irradiance and one for the phase. This makes even numerical solutions difficult. However, we find that the analysis of thin limiters qualitatively describes the operation of thick limiters.

3. CHARACTERISTICS OF SELF-PROTECTING LIMITERS

Our initial experiments on thick limiters were performed in ZnSe using 30 ps (FWHM) pulses of 532 nm wavelength light obtained from a frequency-doubled mode-locked and Q-switched Nd:YAG laser with a single pulse switched out. The experimental arrangement is depicted in Figure 2.

The second lens was used to refocus the transmitted beam through a pinhole, such that the low-energy pinhole transmittance was approximately 90 percent. The energy transmitted through the pinhole was measured on a large-area Si photodiode placed immediately behind the pinhole. The input energy and pulsewidth were simultaneously monitored for each pulse. [10] The incident energy was continuously variable without beam distortion or deviation by using a half-wave plate and polarizer. As the laser repetition rate was 0.5 Hz, the experiments were effectively single shot. The total energy transmittance could be measured by removing the pinhole, thus showing the contribution of nonlinear absorption to the limiting. At high input levels, this was found to be less significant than the fluence limiting caused by self-defocusing. the device showed a linear transmittance for input energies much less than the limiting energy

(E_L) and a constant transmitted fluence for input energies much greater than (E_L). E_L is defined as the input energy at which the transmittance falls to one half of the low-energy transmittance. It should be noted that E_L was not particularly sensitive to the choice or position either of the pinhole or of the refocusing lens. We note that the aperture is used only as a convenient means for monitoring the on axis fluence.

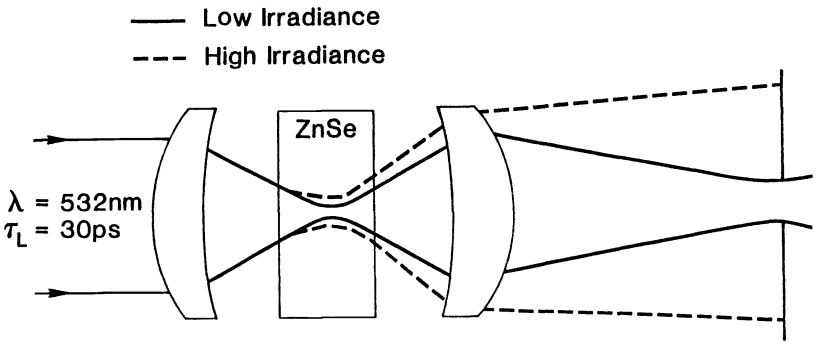

Fig. 2. Configuration for a Self-Protecting Optical Limiter.

The limiting energy and the damage energy, E_D, were measured for various distances ΔZ between the sample front surface and the beam waist. This was done for two sample thicknesses L (L = 10 and 3 mm) and two focusing lenses (f = 37 and 75 mm, producing measured focused spot radii in air of 8 and 14 μm half-width $1/e^2$ maximum, respectively). Figure 3(a) shows the limiting energy as a function of ΔZ for both samples with the f = 37 mm lens. A minimum limiting energy of 14 nJ was observed for the 10-mm sample, and 32 nJ for the 3-mm sample. The limiting energies when focused on the rear surface are similar for both samples. The data for the f = 75 mm lens showed a similar response but with limiting energies between 3 and 5 times greater. For each position ΔZ, the device transmittance was measured for increasing energy until the front surface was damaged.

It is useful to define the dynamic range (DR) of the limiter as the ratio of E_D to E_L. Single-shot damage occurred at a wide range of fluences attributed to variations in surface quality, as the general condition of the surfaces was poor. Assuming that a well prepared surface would give a constant damage fluence (or irradiance), we can show the variation of the DR with ΔZ by using the fact that E_D is directly proportional to the beam area on the front surface of the sample. In Figure 3(b) we show this version of the dynamic range plotted versus ΔZ for the 10-mm-thick sample and 37-mm focal-length lens. This shows that the optimum condition for a large DR is when the focus is as far into the sample as possible (i.e., in this case on the rear face of the sample). Using a previously measured damage threshold, we estimate that with carefully prepared surfaces the maximum dynamic range would be $>10^4$. The dynamic range was also measured for the 3-mm-thick sample with the same lens and the 10-mm-thick sample with a 75-mm focal-length lens. The behavior was similar for all configurations. However, the absolute value of the DR was found to be strongly dependent on the configuration. The 3-mm sample gave a maximum DR that was a factor of 20 smaller than for the 10-mm sample with the same lens. The *f*-number used is an even more important factor in determining the DR. The maximum DR for the 10-mm sample with a 75-mm focusing lens was almost 10^2 smaller than for the 37-mm lens with the same sample.

These results allowed us to conclude that tight focusing and longer sample lengths are clearly advantageous in a low-energy, large-dynamic-range limiter. On the basis of this, we have designed and constructed a monolithic optical power limiter (MONOPOL). This device was fabricated from a single piece of semiconductor with spherically polished ends, so that a collimated input beam focuses inside the medium and is recollimated on leaving it for low input. In choosing this design, we have optimized the dynamic range of the device for the given *f*-number, in that the front surface is as far from the beam waist as is possible.

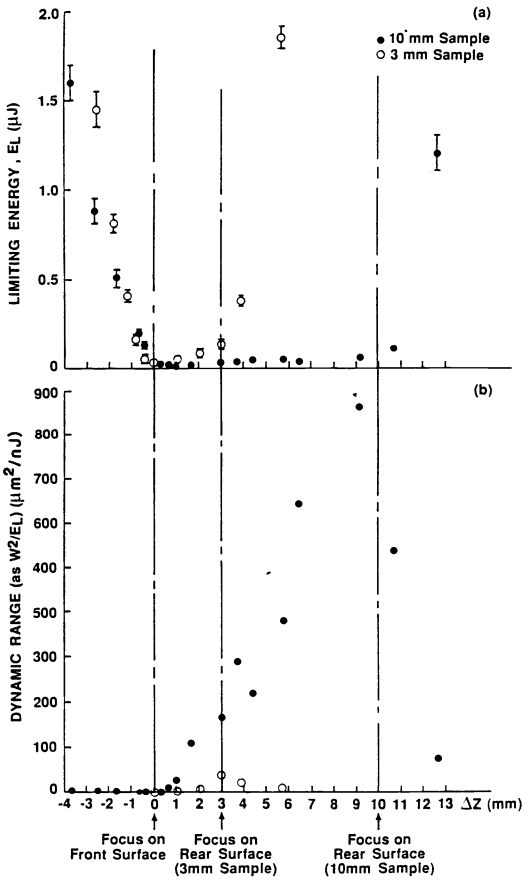

Fig. 3(a). Plot of limiting energy versus position of beam waist relative to the front surface of the sample ΔZ. (b) Dynamic range, plotted as w^2/E_L, where w is the spot size on the front surface of the sample. The true dynamic range (E_D /E_L) is approximately 1.3 times this number.

The MONOPOL was fabricated from chemical-vapor-deposition-grown polycrystalline ZnSe. The ZnSe device had a length of 32 mm and diameter of 12 mm. The performance was determined by placing it in the path of the beam. A further 100-mm focal-length lens was placed at the output of the limiter to focus the output onto a pinhole detector arrangement as in the previous experiments. In this case, the low-energy (1-nJ) pinhole transmittance was ≃65 percent. Thus we are monitoring primarily the output fluence. The limiting input energy, E_L, is 10 nJ, which is within a factor of 2 of the predicted scaling. We have calculated the DR of the ZnSe MONOPOL to be ≃5 x 10^5, using a conservative estimate for the surface-damage threshold of ≃10 GW/cm². The device was not tested to destruction, but it was successfully tested up to input energies of 100 μJ, so that a minimum DR of >10^4 may be confidently stated for 20-psec pulses. From the input energy where the input-output curve first becomes horizontal, up to the maximum

tested energy, the transmitted on-axis fluence changed by only a factor of 3. This corresponds to an average slope $dE_T / dE_{in} \simeq 3 \times 10^{-4}$. The maximum energy transmitted was 3 nJ, while the low energy transmittance was 10 percent.

4. SPATIAL AND TEMPORAL RESPONSE

The spatial distribution of the transmitted fluence was measured for a number of different input energies using a vidicon. The vidicon was placed ≃2.8m behind the ZnSe device (toward the far field) we see the fluence-limiting characteristics of Figure. 4(b). Here the temporally integrated spatial energy distribution is shown as a function of position for input energies from 13 nJ to 61 μJ. For the data shown, no filters were changed in front of the vidicon. As the input energy is increased, the energy simply gets spread out in space, limiting the fluence and thus protecting the sensitive vidicon photocathode. If we look just at the on-axis portion of this light through a 0.4 mm aperture, we get the input-output characteristics shown in Figure 4 (a).

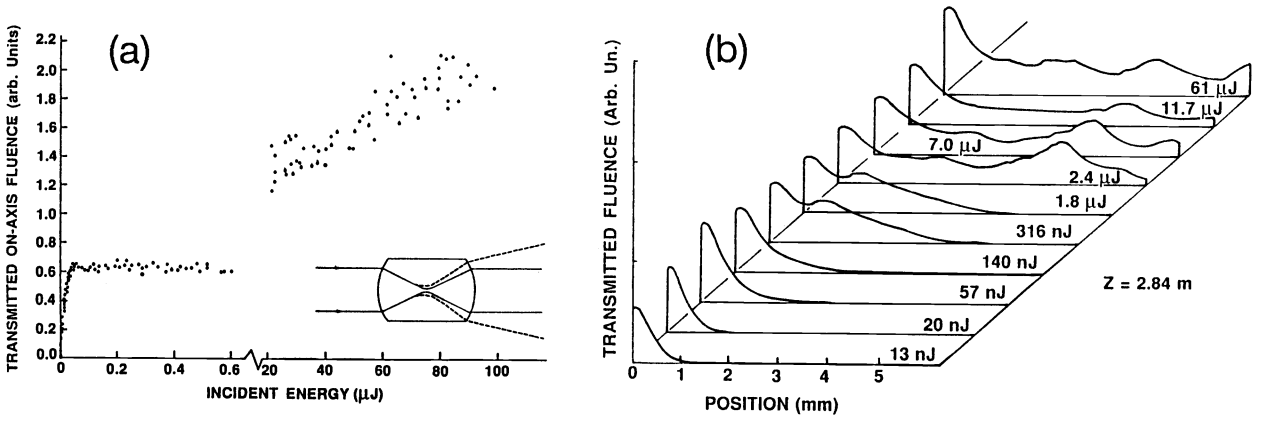

Fig. 4. (a) Input-output characteristic for the ZnSe MONOPOL (note change of scale). The transmittance changes by a factor of 3 between the turnover energy and the maximum tested energy. Inset: Schematic of the MONOPOL. The beam focuses in the center. (b) Transmitted fluence at 2.8m behind the ZnSe monolithic limiter as detected by a vidicon as a function of position at various input energies.

Sending the pulse through the limiter onto the entrance slit of a 2-psec-resolution streak camera allows us to look at the spatial and temporal energy distribution simulatenously on the vidicon screen. What we see at low inputs, shown in Figure 5 (a), is the Gaussian spatial distribution and a nearly Gaussian distribution in time. At higher input, Figure 5(b), as the pulse develops, the energy spreads out in space into two wings. This is clearly advantageous from the standpoint of protecting optical components.

5. SCALING RULES

The effect of nonlinear beam distortion inside the nonlinear medium itself makes a detailed theoretical analysis of self-protecting thick limiters difficult. No analytical solution of the nonlinear wave equation is known for this problem, and a numerical solution is extremely complicated. For these reasons, we have made some relatively simple approximations which allow us to predict how thick limiters will behave for longer pulsewidths, how will they work at other wavelengths, and how well other direct-gap semiconductors with smaller bandgaps will work as limiters in the infrared.

In what follows, we assume that at the limiting threshold, the beam is not strongly distorted by nonlinear effects, and that the beam is therefore still essentially a Gaussian in the region of the focus. The limiting in the far field is thus caused by only a nonlinear phase distortion $\Delta\phi$, in this focal region. We assume that at the limiting threshold, the nonlinearly induced phase change Δn_L caused by a refractive index change Δn is $\Delta\phi \simeq 2\pi$. Since $\Delta\phi = 2\pi\ \Delta n\ L_{eff}\ /\lambda$, this gives $\Delta n_L \simeq \lambda/L_{eff}$. Now for a thick limiter, the effective interaction length, L_{eff}, is that length over which the beam remains intense. Thus, $L_{eff} \propto z_0$, where z_0 is the confocal beam parameter, $\pi w_0^2/\lambda$, where w_0 is the $1/e^2$ beam radius at the beam waist, this leads to $\Delta n_L \propto \lambda^2/w_0^2$.

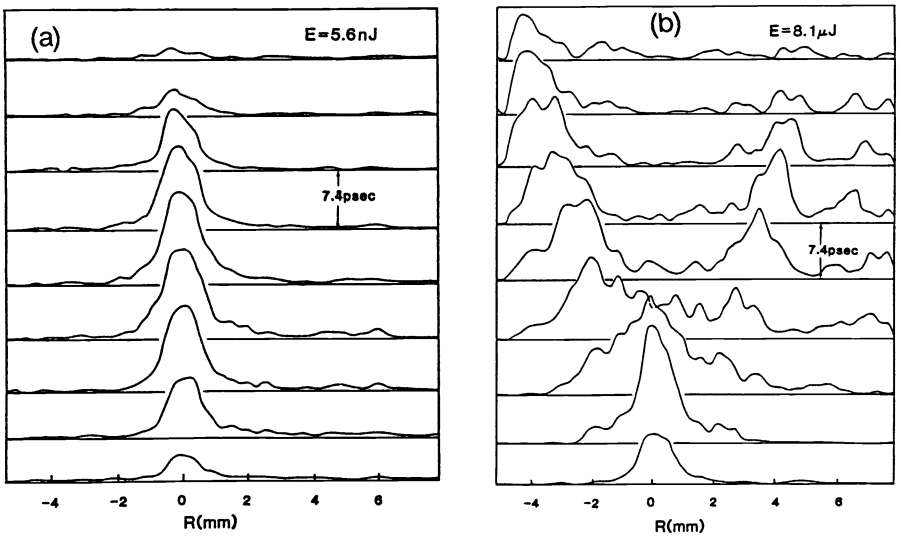

Fig. 5. (a) Spatial energy distribution at 2.8m behind the ZnSe monolithic limiter at various times as detected by a streak-camera-vidicon system for an input energy of 5.6 nJ. (b) Same as (a) for an input energy of 8.1 μJ.

The refractive index change, Δn, is in proportion to the number of photo-generated carriers, N. This has been shown to be true [3] at least in the case of low to moderate carrier densities, which is appropriate for the modelling of the onset of limiting. We have used two models for this nonlinear refraction, the "plasma generation" model of Auston et al. [11] and a slightly more sophisticated band filling or "Moss-Burstein shift" first proposed by Moss [12] and later developed by Miller et al [3]. Both give remarkably similar results so we shall concentrate on Auston's model for the purpose of demonstration. This yields

$$\Delta n \propto N \frac{E_g}{(\hbar\omega)^2} \frac{1}{1-(\hbar\omega/E_g)^2} \tag{1}$$

where E_g is the semiconductor energy gap, and material independent and frequency independent constants have been incorporated into the constant of proportionality for simplicity. The carrier density is given by

$$N(t) = \frac{\beta_2}{2\hbar\omega} \exp(-t/\tau_R) \int_{-\infty}^{t} I^2(t') \exp(t'/\tau_R)\, dt' = \frac{\beta_2}{\hbar\omega} G(I,\tau_R) \tag{2}$$

where we have used $G(I,\tau_R)$ to represent a (frequency independent) carrier generation function, τ_R is the carrier recombination time and β_2 is the two photon absorption coefficient, $\beta_2 \propto F_2(2\hbar\omega/E_g)/E_g^3$ and $F_2(x) = (x-1)^{3/2}/x^5$. These two-photon absorption relationships have previously been experimentally verified. [2]

Combining the above relations gives:

$$\Delta n(t) \propto G(I,\tau_R)\ \frac{E_g}{(\hbar\omega)^8}\ \frac{(2\hbar\omega/E_g-1)^{3/2}}{1-(\hbar\omega/E_g)^2} \tag{3}$$

This is shown as a function of photon energy for the semiconductor ZnSe (E_g = 2.67 eV) in Figure 6 below.

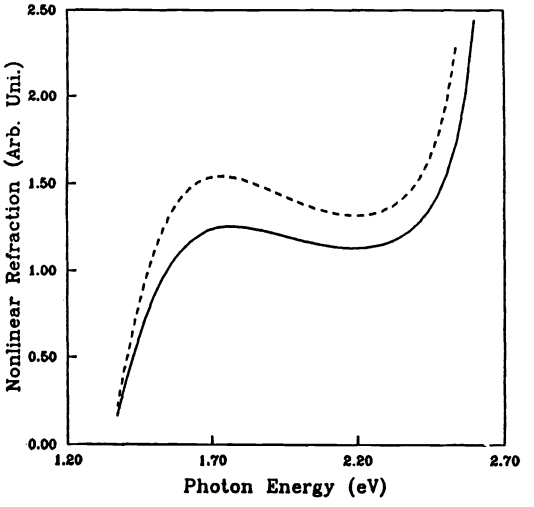

Fig. 6. Nonlinear refraction by two-photon excited carriers, calculated by Auston model (dotted line) and by Moss-Burstein shift (solid line).

Remarkably, this somewhat complicated function gives an extremely flat response in the region of 2PA ($E_g < 2\hbar\omega < 2E_g$). This is as expected, since above the two-photon resonance the efficiency of 2PA starts to decrease, while the excited carrier refractive index increases with frequency. The result is a flat response and Δn varies by less than ±25% in the range $0.57 < (\hbar\omega/Eg) < 0.94$, corresponding to $500 < \lambda < 810$ nm for ZnSe. For shorter wavelengths, Δn becomes very large as the bandgap resonance is approached, but here the linear absorption is also large, so that there is no application for power limiting in that wavelength region.

We may use the above result to simplify our scaling to other semiconductor/wavelength combinations. If we make the reasonable assumption that the limiter will be operated in the "flat" region defined above, then we can remove all terms in ($\hbar\omega$/Eg) from the formula for Δn given in equation 3. Thus,

$$\Delta n(t) \propto G\ (I,\ \tau_R)\ \frac{1}{(\hbar\omega)^7}\ \propto G\ (I,\ \tau_R)\ E_g^{-7}, \tag{4}$$

since we always choose a suitable semiconductor bandgap for the particular optical frequency, ω, and within the operating range $\hbar\omega/E_g$ acts as a constant. Now $\Delta n_L \propto \lambda^2/w_0^2$ so that $G_L\ (I,\tau_R) \propto E_g^{7}\ \lambda^2/w_0^2$, where G_L is the value of the carrier generation function at limiting. However, $\lambda \propto (\hbar\omega)^{-1} \propto E_g^{-1}$ in our case, giving, $G_L \propto E_g^{5}\ w_0^{-2}$. The calculation of the carrier generation function is simplified in two limits. (i) $\tau_R >> \tau_p$, where τ_p is the pulsewidth, i.e., the short pulse limit, and (ii) $\tau_R << \tau_P$, the long pulse limit. For the short pulse limit, we can ignore recombination, and $G_L\ (t\simeq\infty) \propto I_L^{2}\ \tau_p$, where I_L is the peak limiting irradiance which can now be given by

$$I_L \propto \frac{(E_g)^{5/2}}{w_0\sqrt{\tau_p}}, \tag{5a}$$

and thus, the limiting energy is determined by

$$E_L \propto (E_g)^{5/2}\, w_0 \sqrt{\tau_p}\ . \tag{5b}$$

Note that for longer pulses, carrier generation is more efficient and I_L decreases, however, E_L increases as the square root of the pulsewidth. In the long pulse limit, the performance is expected to be degraded by the effects of carrier recombination. In this case, $G(t) \propto I^2(t)\tau_R$, so that the peak limiting irradiance and energy are

$$I_L \propto \frac{(E_g)^{5/2}}{w_0\sqrt{\tau_R}}, \tag{6a}$$

and

$$E_L \propto (E_g)^{5/2}\, w_0\, \frac{\tau_p}{\sqrt{\tau_R}}\ . \tag{6b}$$

Note that performance is reduced from the short pulse limit by a factor of $(\tau_p / \tau_R)^{1/2}$. Otherwise, the scaling is identical.

Clearly then, narrow-gap semiconductor limiters should work in the infrared much better than the ZnSe visible limiter we tested. There is, however, one further restriction in that the focused spot size for any given f-number optics is proportional to λ, i.e., $w_0 \propto E_g^{-1}$. Thus, in the case of diffraction-limited focusing we have

$$E_L \propto (E_g)^{3/2} \sqrt{\tau_p} \qquad \text{(short pulse limit)}\ , \tag{7}$$

and

$$E_L \propto (E_g)^{3/2}\, \frac{\tau_p}{\sqrt{\tau_R}} \qquad \text{(long pulse limit)}\ . \tag{8}$$

6. COMPARISON OF SCALING RULES WITH NANOSECOND AND INFRARED DATA

In addition to ZnSe with 532 nm picosecond pulses, a number of other limiting experiments have been performed. In this section, we will compare our results of limiting in ZnSe with longer pulses, and with other materials at appropriately longer wavelengths.

First, the ZnS monolithic limiter was tested using 532 nm picosecond pulses. Applying equation (4), our scaling rules indicate that the limiting energy should be a factor of $[E_g\,(ZnS)/E_g\,(ZnSe)]^7$ larger than E_L for ZnSe, as in this case the wavelengths are the same. This gives a factor of 9·1, indicating an E_L of 91 nJ. In fact, the measured limiting energy for the ZnS monolithic limiter was 120 nJ, in reasonable agreement with the calculation.

Limiting experiments were also performed in a 10mm thick sample of ZnSe with nanosecond pulses of 532 nm light. The limiting energy is shown in Figure 7 as a function of position of the beam waist along z.

Comparing with the psec results when the waist is in the middle of the sample, we see that the nanosecond pulses produce a limiting energy of 2 μJ, as opposed to 40 nJ for psec pulses. The appropriate equation for the picosecond data is (5b), whereas for the nanosecond data the long pulse approximation,equation (6b), is more appropriate. Substituting for τ_p, w_0 in each of these equations, and assuming a 1 ns recombination time, we estimate E_L (nsec) $\simeq$ $40E_L$ (psec) $\simeq$1.6 μJ, again in good agreement. We estimate the 1 nsec recombination time from our degenerate four wave mixing experiment.

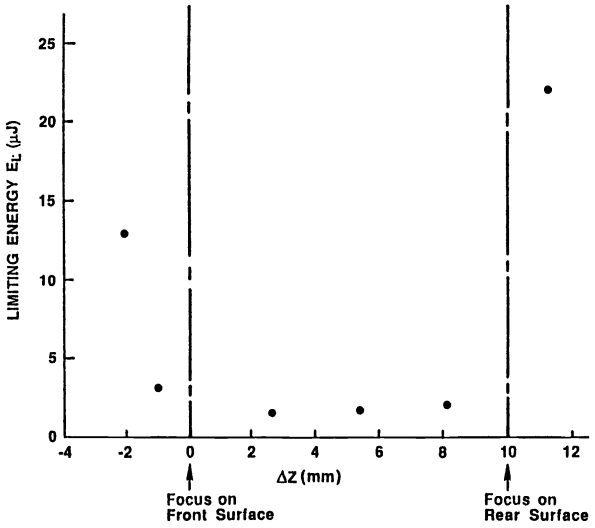

Fig. 7. Limiting energy as a function of waist position inside a 10mm thick ZnSe polycrystalline sample. λ = 532 nm, τ_p = 20 ns (FWHM) and w_0 = 3.2 μm.

Limiting at 1.06 μm with picosecond pulses was also observed in CdTe (see Figure 8) . This sample was 3mm thick, so we compare our data with the data obtained in thick ZnSe. To make this comparison, we apply equation (5b) as the short pulse limit is valid for both cases. Accounting for the different spot sizes, pulsewidths and energy gaps, the predicted limiting energy in CdTe is 27 nJ, whereas we measured $E_L \simeq$ 35 nJ, again in very close agreement.

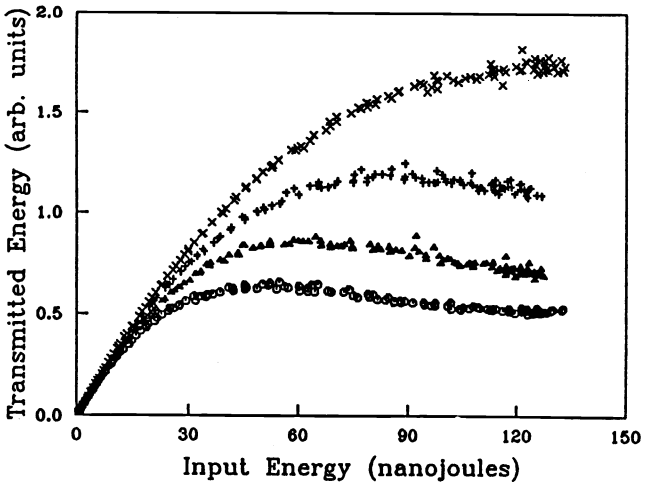

Fig. 8. Limiting curves for CdTe with 45 ps (FWHM) pulses of 1.06 μm light and a spot size $w_0 \simeq$ 11 μm. o - ΔZ = 0; Δ - ΔZ = 0.73 mm; + - ΔZ = 1.27 nm; x - ΔZ = 1.82 mm.

In Figure 9, we show limiting curves for InSb with 10.6 μm wavelength light from a CO_2 laser. This experiment involved a rather different experimental configuration than the previous data. The spot size was 60 μm and the sample length was 1mm, so that the limiter was not truly "thick". The observed limiting energy, using an aperture in the beam to detect on axis fluence, was 4 μJ with a 170 ns (HW1/eM) pulsewidth. It was decided to compare this with the nanosecond ZnSe data, as both results are in the same long pulse limit, and equation (6b) applies to both cases. However, scaling was difficult to do in this case, as the limiter was not thick, and there were difficulties in predicting the recombination time, which is almost certainly carrier-density dependent. Using a best-guess of $\simeq$ 5 ns for the recombination time, and $L/L_{eff} \simeq 4$, we obtain a scaled E_L of 0.6 μJ, considerably smaller than the 4 μJ observed. Although this result is probably good to within one order of magnitude, the uncertainties make the scaling unreliable in this case. It is worth noting that we are extrapolating both the 2PA coefficient and the nonlinear refraction over three orders of magnitude, while assuming that there is no excited state absorption, to obtain this result.

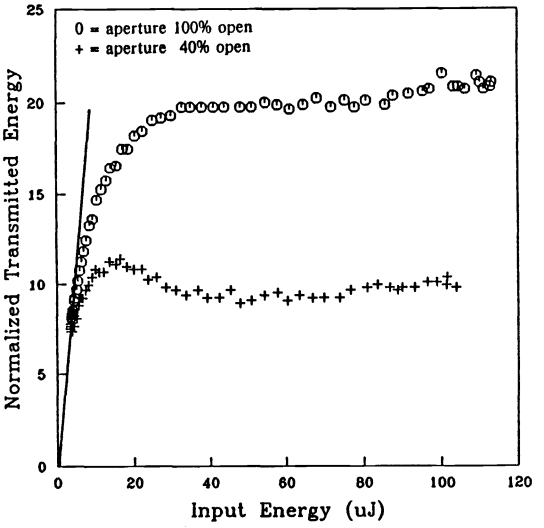

Fig. 9. Input-Output curves for 1mm thick InSb at room temperature, with 10.6 μm radiation.

7. CONCLUSION

We have built and characterized limiters for the visible which exhibit very low limiting energies. Limiting energies (powers) as low as 10 nJ (300 Watts) for picosecond pulses and 2 μJ (80 Watts) for nanosecond pulses have been measured. We have shown how theory predicts that these limiters should be very broad band, and should work better (i.e. lower threshold) using narrow gap semiconductors in the infrared. We have developed simple scaling rules to predict performance at longer wavelengths in appropriate narrow gap semiconductors, and for longer pulses. Initial experiments have verified these scaling rules.

8. ACKNOWLEDGEMENTS

The authors wish to acknowledge the support of DARPA/CNVEO, the Florida High Technology and Industrial Council and the National Science Foundation grant ECS #8617066.

9. REFERENCES

1. S.A. Akhmanov, R.V. Khokholov and A.P. Sukhorukov, "Self-focusing, self-defocusing, and self-modulation of laser beams" in *laser Handbook*,F.T. Arecchi and E.O. Schulz-Dubois eds. (North-Holland, Amsterdam,1972) Vol. 2, pp. 1151-1228.

2. E.W. Van. Stryland,H. Vanherzeele, M.A. Woodall, M.J. Soileau, A.L. Smirl, S. Guha and T. F. Boggess, Opt. Eng. **24,** 613 (1985).

3. D.A.B. Miller, C.T. Seaton, M.E. Prise and S.D. Smith, Phys. Rev. Lett. **47,** 197 (1981)

4. J.E. Geusic, S. Singh, D.W. Tipping, and T.C. Rich, Phys. Rev. Lett. **19,** 1126 (1969)

5. T.F. Boggess, S.C. Moss, I.W. Boyd, and A.L. Smirl, Opt. Lett. **9,** 291 (1984)

6. J.M. Ralston and K.R. Chang, Appl. Phys. Lett. **15,** 164 (1969).

7. A.C. Walker, A.K. Kar, Wei Ji, U. Keller, and S.D. Smith, Appl. Phys. Lett. **48,** 683 (1986).

8. T.F. Boggess, A.L. Smirl, S.C. Moss, I.W. Boyd, and E.W. Van Stryland, IEEE J. Quantum Electron. **QE-21,** 488 (1985).

9. D.J. Hagan, E.W. Van Stryland, M.J. Soileau, and Y.Y. Wu, Opt. Lett. **13,** 315 (1988).

10. E.W. Van Stryland, Opt. Commun. **31,** 93 (1979).

11. D.H. Auston, S. McAffee, C.V. Shank, E.P. Ippen, and O. Teschke, Solid State Electron. **21,** 147 (1978).

12. T.S. Moss, Phys. Stat. Sol. **B101,** 555 (1980).